Topologically Protected Quantum Coherence in a Superatom

Wei Nie,[1,2] Z. H. Peng,[3] Franco Nori,[4,5] and Yu-xi Liu[1,2,*]
[1]Institute of Microelectronics, Tsinghua University, Beijing 100084, China
[2]Frontier Science Center for Quantum Information, Beijing, China
[3]Key Laboratory of Low-Dimensional Quantum Structures and Quantum Control of Ministry of Education, Key Laboratory for Matter Microstructure and Function of Hunan Province, Department of Physics and Synergetic Innovation Center for Quantum Effects and Applications, Hunan Normal University, Changsha 410081, China
[4]Theoretical Quantum Physics Laboratory, RIKEN Cluster for Pioneering Research, Wako-shi, Saitama 351-0198, Japan
[5]Physics Department, The University of Michigan, Ann Arbor, Michigan 48109-1040, USA

(Received 24 January 2019; revised manuscript received 1 October 2019; published 16 January 2020)

Exploring the properties and applications of topological quantum states is essential to better understand topological matter. Here, we theoretically study a quasi-one-dimensional topological atom array. In the low-energy regime, the atom array is equivalent to a topological superatom. Driving the superatom in a cavity, we study the interaction between light and topological quantum states. We find that the edge states exhibit topology-protected quantum coherence, which can be characterized from the photon transmission. This quantum coherence helps us to find a superradiance-subradiance transition, and we also study its finite-size scaling behavior. The superradiance-subradiance transition also exists in symmetry-breaking systems. More importantly, it is shown that the quantum coherence of the subradiant edge state is robust to random noises, allowing the superatom to work as a topologically protected quantum memory. We suggest a relevant experiment with three-dimensional circuit QED. Our study may have applications in quantum computation and quantum optics based on topological edge states.

DOI: 10.1103/PhysRevLett.124.023603

Introduction.—One of the most striking achievements in modern physics is the discovery of topological materials. Also, novel forms of topological quantum states are pursued in both matter and light [1–4]. These exotic states are protected by band gaps which can be closed via topological phase transitions [5–7]. Topological quantum states have applications in many quantum technologies, e.g., topological qubits [8–12], topological quantum channels [13,14], topological surface waves [15,16], and topological lasing [17–20]. In topological many-body systems, owing to the peculiar geometry of edge states, driving a single atom could excite an edge state and generate a quantum nonlinearity for photons [21]. In the emerging field of topological quantum optics [21–25], the interaction between light and topological quantum states should be explored to better understand the properties of topological quantum matter.

Collective behavior in quantum many-body systems originates from quantum coherence [26]. In cavity QED, single-photon absorption is able to build many-body coherence among atoms, producing superradiance or subradiance [27–31]. A superatom model is used to explain such collective phenomena [32] and has been realized via Rydberg blockade [33,34]. Recent studies about topological matter show that single-atom quantum coherence can be protected by topology [35–38]. Indeed, topological protection makes nonlocal quasiparticles in the ground state manifold ideal candidates for realizing topological quantum computation [39,40]. In particular, researchers have analyzed quantum coherence of Majorana zero modes in decoherence-free subspaces [41] and quantum manipulation of Majorana bound states via electron-photon interactions [42–45].

We consider a quasi-one-dimensional (1D) topological array of two-level atoms. In the low-energy regime, the atom array has a ground state and a single-excitation subspace which has many bulk states and two edge states. The large gaps between edge states and bulk states in the single-excitation subspace help us to define a topological superatom, which consists of a ground state and two edge states. The typical features of edge states make them experimentally measurable in various topological systems [46–50]. Here, we study edge states via light-matter interactions, from which topology-protected quantum coherence is found. Superconducting quantum circuits have applications in quantum computation and microwave photonics [51,52]. The recent development of quantum chip technologies makes it possible to address qubit arrays, e.g., via 3D integration [53–56]. For concreteness, here we propose an experimental setup for studying topological mater in an integrated superconducting quantum chip.

3D circuit QED with a topological atom array.—Figure 1(a) shows the schematic of a 3D circuit QED with multilayer fabrication process. The top layer consists of a

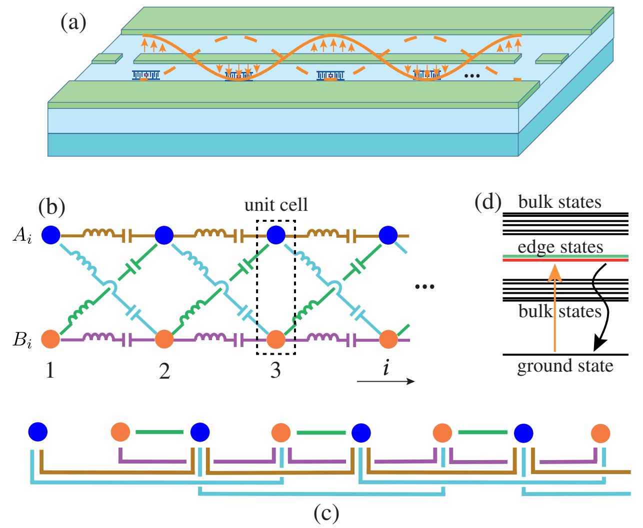

FIG. 1. (a) Schematic of a 3D circuit QED. The top layer contains a microwave transmission line resonator, which plays the role of cavity, coupled with an array of superconducting artificial atoms. On the bottom layer, superconducting coplanar waveguides are fabricated and coupled to the atoms on the top panel via interconnects in the middle dielectric layer (see Ref. [64] for details). (b) The atom array in (a) has internal interactions between neighboring unit cells. The atoms are coupled by resonators represented by LC circuits. Blue and orange dots denote atoms A and B in unit cells. (c) Wiring of the coupling circuits, so a 1D atom array can be obtained and coupled to the transmission line resonator, as shown in (a). (d) Optically addressing edge states of the topological atom array.

transmission line resonator interacting with an artificial atom array. In the bottom layer, superconducting coplanar waveguides are fabricated (not shown). The atom array has a ladder configuration, as shown in Fig. 1(b). The couplings between neighboring unit cells are realized by LC resonators. Through 3D wiring, the ladder structure of the atom array can be reconfigured as a 1D array, as shown in Fig. 1(c). The crossings between wires represent airbridges [57–59]. To show how the atoms are coupled, we first consider the interaction between atoms A_1 and B_2 in the first and second unit cells, respectively. In the rotating frame with the frequency of the coupler, the system Hamiltonian becomes ($\hbar = 1$)

$$H_{AB} = \sum_{\alpha=1A,2B} \Delta_\alpha \sigma_\alpha^+ \sigma_\alpha^- - g_\alpha(\sigma_\alpha^+ \hat{a}_1 + \hat{a}_1^\dagger \sigma_\alpha^-), \qquad (1)$$

where Δ_α and g_α are detunings and couplings between the atoms and the LC resonator, respectively. Hereafter, we assume $\Delta_{1A} = \Delta_{2B} = \Delta$. Also, $\sigma_{1A}^+ = |A_1\rangle\langle\alpha_1|$ and $\sigma_{2B}^+ = |B_2\rangle\langle\beta_2|$ are the atomic operators where $|\alpha_1\rangle$ ($|A_1\rangle$) and $|\beta_2\rangle$ ($|B_2\rangle$) denote the ground (excited) states of atoms A_1 and B_2, respectively. And $\hat{a}_1$ ($\hat{a}_1^\dagger$) represents the annihilation (creation) operator of the resonator. When $g_{1A}, g_{2B} \ll |\Delta|$, by making a Schrieffer-Wolff transformation, we can obtain the effective Hamiltonian

$$\tilde{H}_{AB} = \left(\Delta + \frac{g_{1A}^2}{\Delta}\right)\sigma_{1A}^+\sigma_{1A}^- + \left(\Delta + \frac{g_{2B}^2}{\Delta}\right)\sigma_{2B}^+\sigma_{2B}^- + \frac{g_{1A}g_{2B}}{\Delta}(\sigma_{1A}^+\sigma_{2B}^- + \sigma_{2B}^+\sigma_{1A}^-). \qquad (2)$$

The first and second terms contain Lamb shifts due to the virtual photons in the LC resonator. The last term is the effective coupling between these two atoms, which can be realized in many quantum systems [60–63]. To couple two neighboring unit cells, we need four LC resonators, each one producing a specific interaction. Based on this coupling scheme, an atom array can be obtained [64].

Topological superatom.—The atomic interactions produced by exchanging virtual photons allow the study of many-body phenomena [65–67]. Using the airbridge wiring technique [57–59], quantum networks of artificial atoms can be realized in superconducting quantum circuits. Considering the lattice in Fig. 1(b), the effective Hamiltonian of the atom array can be written as

$$\tilde{H} = \sum_{i=1}^{N} \delta(\sigma_{iA}^+\sigma_{iA}^- - \sigma_{iB}^+\sigma_{iB}^-) + \sum_{i=1}^{N-1}[t_p(\sigma_{iA}^+\sigma_{i+1A}^- - \sigma_{iB}^+\sigma_{i+1B}^-) - t_c(\sigma_{iA}^+\sigma_{i+1B}^- - \sigma_{iB}^+\sigma_{i+1A}^-) + \text{H.c.}], \qquad (3)$$

where δ is half of the effective energy splitting between two excited states $|A_i\rangle$ and $|B_i\rangle$ of atoms A and B in the ith unit cell; t_p and t_c are, respectively, the parallel and cross-couplings [64]. To better see the physical picture of Eq. (3), we can rewrite it in the single-excitation subspace $\{|\mathcal{A}_i\rangle, |\mathcal{B}_i\rangle\}$, with $|\mathcal{A}_i\rangle = \sigma_{iA}^+|G\rangle$ and $|\mathcal{B}_i\rangle = \sigma_{iB}^+|G\rangle$ (here $|G\rangle = |\alpha_1\beta_1\alpha_2\beta_2\cdots\rangle$), which represents a lattice as shown in Fig. 2(a). After making Fourier transforms to the vectors $|\mathcal{A}_i\rangle$ and $|\mathcal{B}_i\rangle$, Eq. (3) can be written in crystal momentum space as $\tilde{H}(k) = \sum_k \Psi_k^\dagger h(k)\Psi_k$, with $\Psi_k^\dagger = (|\mathcal{A}_k\rangle, |\mathcal{B}_k\rangle)$, and

$$h(k) = d_y(k)\sigma_y + d_z(k)\sigma_z. \qquad (4)$$

Here, $d_y(k) = 2t_c \sin k$ and $d_z(k) = \delta + 2t_p \cos k$. The system is protected by chiral symmetry [68], i.e., $\sigma_x h(k)\sigma_x = -h(k)$, as well as particle-hole and time-reversal symmetries, and belongs to the BDI class [69]. The topological nature can be extracted from the winding number [70,71], defined in the auxiliary space $[d_y(k), d_z(k)]$, as shown in Fig. 2(b). When $-\delta_c < \delta < \delta_c$, with $\delta_c = 2|t_p|$, the system is in a topological insulating phase with nontrivial winding number. As $|\delta|$ increases and becomes larger than δ_c, a normal insulator is obtained for zero winding number.

From the edge-bulk correspondence, it is known that the topological phase supports edge states for open boundary conditions. The energy spectrum of the atom array in the single-excitation subspace is shown in Fig. 2(c). Zero modes for $|\delta| < \delta_c$ represent edge states. The edge states localized at the left and right boundaries are

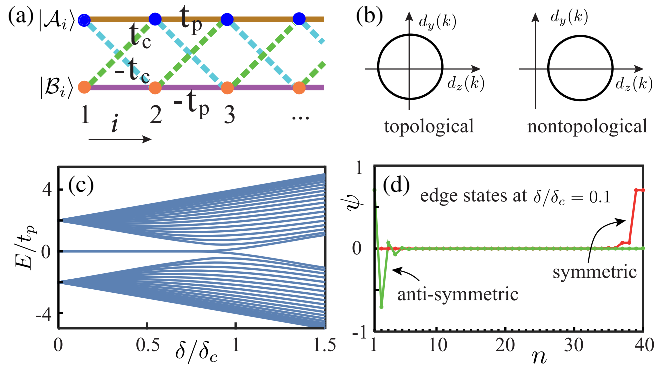

FIG. 2. (a) Lattice in the single-excitation subspace. Solid and dashed lines represent parallel and cross-couplings, respectively. (b) Topology of the lattice in the auxiliary space $[d_y(k), d_z(k)]$. The winding number for the topological phase is nontrivial. (c) Energy spectrum of the tight-binding lattice in (a). There are large gaps between edge states and bulk states. As δ changes across the critical point δ_c, edge states undergo a transition to bulk states. (d) Wave functions of edge states at $\delta = 0.1\delta_c$. Here n labels the positions of atoms in the array, and odd (even) number of n corresponds to $|\mathcal{A}_{(n+1/2)}\rangle$ ($|\mathcal{B}_{(n/2)}\rangle$). The parameters in (c) and (d) are $t_c = t_p$ and the number of unit cells $N = 20$.

$$\psi_L = [\mathcal{N}_L^-]^{-\frac{1}{2}} \sum_i [(\lambda_{-,1})^i - (\lambda_{-,2})^i]\phi_-^{(i)}, \tag{5}$$

$$\psi_R = [\mathcal{N}_R^+]^{-\frac{1}{2}} \sum_i [(\lambda_{-,1})^{N+1-i} - (\lambda_{-,2})^{N+1-i}]\phi_+^{(i)}, \tag{6}$$

where $\mathcal{N}_L^-$ and $\mathcal{N}_R^+$ are the renormalization factors and $\lambda_{-,l} = [\delta + (-1)^{l-1}(\delta^2 - 4t_p^2 + 4t_c^2)^{1/2}]/(-2t_c - 2t_p)$ (with $l = 1, 2$) [11,72], $\phi_\pm^{(i)} = |\mathcal{A}_i\rangle \pm |\mathcal{B}_i\rangle$. From the edge states, we can find several features. First, the left and right edge states are polarized with antisymmetric and symmetric superpositions of $|\mathcal{A}_i\rangle$ and $|\mathcal{B}_i\rangle$, respectively. Second, the edge states are exponentially localized in the boundaries, as shown in Fig. 2(d). These properties are helpful for manipulating edge states. The above edge states occur when $|\lambda_{-,l}| < 1$. The case $|\lambda_{-,l}| > 1$ has oppositely polarized edge states [64]. From the spectrum, we can find that the edge states have large energy gaps with bulk states. Therefore, a topological superatom with a V-shaped three-level structure [73,74], which consists of a ground state and two edge states, can be modeled to characterize the atom array in its low-energy regime.

Optically probing edge states.—Generally speaking, it is challenging to selectively drive quantum many-body states in large-scale systems. However, owing to specific properties of the edge states analyzed above, one can realize interactions between light and edge states. As shown in Fig. 1(a), the atom array can be driven by a single-mode cavity field. The Hamiltonian of the cavity field with external driving is $H_c = \Delta_c \hat{f}^\dagger \hat{f} + i\eta(\hat{f}^\dagger - \hat{f})$, where $\Delta_c = \omega_c - \omega_l$, $\hat{f}$ ($\hat{f}^\dagger$) is annihilation (creation) operator of the cavity field, η is the pumping strength, and ω_c and ω_l are the frequencies of the cavity and driving fields, respectively. The Hamiltonian describing the couplings between the cavity field and the atom array is $H_I = \sum_i(\xi_{iA}\hat{f}\sigma_{iA}^+ + \xi_{iB}\hat{f}\sigma_{iB}^+ + \text{H.c.})$. We consider the resonant driving of edge states, and the large gaps between edge states and bulk states prevent bulk states from being excited. The dynamics of the many-body system is described by the master equation $\dot{\rho} = i[\rho, H_{\text{tot}}] + \mathcal{L}_c[\rho] + \mathcal{L}_a[\rho]$, with the total Hamiltonian $H_{\text{tot}} = \tilde{H} + H_c + H_I$, and dissipation terms for the cavity $\mathcal{L}_c[\rho] = \kappa(2\hat{f}\rho\hat{f}^\dagger - \hat{f}^\dagger\hat{f}\rho - \rho\hat{f}^\dagger\hat{f})$ and atom array $\mathcal{L}_a[\rho] = \sum_{i,\mu,\nu}\gamma_{\mu\nu}(2\sigma_{i\mu}^-\rho\sigma_{i\nu}^+ - \sigma_{i\mu}^+\sigma_{i\nu}^-\rho - \rho\sigma_{i\mu}^+\sigma_{i\nu}^-)$. Here, κ is the decay rate of the cavity, and $\gamma_{\mu\nu}$ the decay rates of the atoms [75]. Specifically, γ_{AA}, γ_{BB} are the decay rates of atoms A_i and B_i, respectively. For simplicity, we write $\gamma_{AA} = \gamma_{BB} = \gamma$. The correlated decays γ_{AB} and γ_{BA} between atoms A_i and B_i play fundamental roles in many quantum optical effects [76–81]. The symmetric correlated decays, i.e., $\gamma_{AB} = \gamma_{BA}$, can be realized by coupling two atoms to a waveguide [82–84]. In the 3D integrated circuits [see Fig. 1(a)], the artificial atoms are coupled to superconducting coplanar waveguides via interconnects [64].

In the low-excitation limit, the dynamic equations of the system are

$$\left\langle \frac{d}{dt}\hat{f} \right\rangle = -(\kappa + i\Delta_c)\langle\hat{f}\rangle - i\Xi^{\text{T}}\langle\boldsymbol{\sigma}\rangle + \eta, \tag{7}$$

$$\left\langle \frac{d}{dt}\boldsymbol{\sigma} \right\rangle = -i(\boldsymbol{\Delta} + \boldsymbol{D} - i\boldsymbol{\Gamma})\langle\boldsymbol{\sigma}\rangle - i\Xi\langle\hat{f}\rangle, \tag{8}$$

where $\boldsymbol{\Xi}$ is the coupling vector between cavity field and atoms. Also, $\langle\boldsymbol{\sigma}\rangle = (\langle\sigma_{1A}^-\rangle, \langle\sigma_{1B}^-\rangle, \langle\sigma_{2A}^-\rangle, \langle\sigma_{2B}^-\rangle, \cdots)^{\text{T}}$, $\boldsymbol{\Delta} = \text{Diag}(\delta, -\delta, \delta, -\delta, \cdots)$, while $\boldsymbol{D}$ and $\boldsymbol{\Gamma}$ denote the couplings and dissipations in the atom array [64]. From Eqs. (7) and (8), the transmission can be formulated as

$$T = \left| \frac{\kappa}{\kappa + i\Delta_c - i\chi} \right|^2, \tag{9}$$

where the susceptibility is $\chi = \boldsymbol{\Xi}^{\intercal}(\boldsymbol{\Delta} + \boldsymbol{D} - i\boldsymbol{\Gamma})^{-1}\boldsymbol{\Xi}$. When the cavity field is resonant with the superatom and the coupling parameters are appropriately chosen, only the edge state can be driven. It is known that in cavity QED with a single atom, the photon transmission exhibits radiation properties of the atom [85,86]. For the topological superatom here, properties of edge states can be explored. Figure 3(a) presents the transmission corresponding to the left and right edge states for $\delta = 0.1\delta_c$. As the correlated decay γ_{AB} increases, the transmission for the left edge state at resonance decreases. However, for the right edge state, the transmission is enhanced accordingly. The cavity decay κ plays an important role in the transmission. Here we consider the cavity with low decay, i.e., $\kappa = 0.1\gamma$. The large cavity decay is also studied [64]. Light

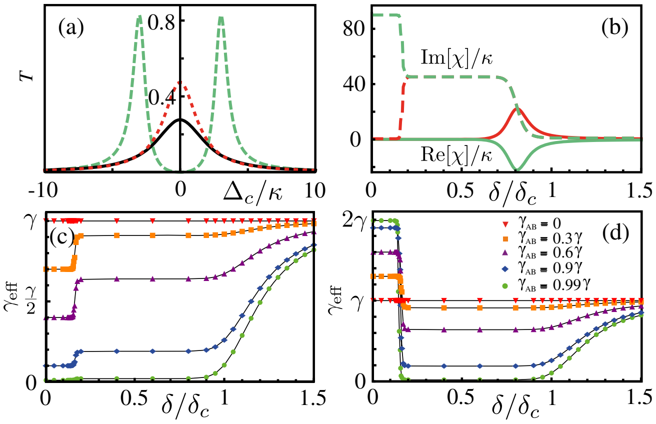

FIG. 3. (a) Transmission of light through the left (green-dashed) and right (red-dotted) edge states with $\gamma_{AB} = 0.99\gamma$. The black curve represents the transmission for both left and right edge states with $\gamma_{AB} = 0$. Here we consider $\delta = 0.1\delta_c$. (b) Real (solid) and imaginary (dashed) parts of the rescaled susceptibility χ by κ for the left (green) and right (red) edge states with $\gamma_{AB} = 0.99\gamma$. $\mathrm{Im}[\chi]$ shows the edge-bulk transition in a finite lattice. (c,d) Variations of coherence when the system is changed from the topological to the non-topological regime. The effective decays of (c) and (d) in the unhybridized regime $\delta < 0.15\delta_c$ correspond to the left and right edge states, respectively. The γ_{AB} used in (c) is the same as that in (d). Other parameters for these figures: $t_c = t_p$, $\gamma = 10\kappa$, $N = 20$.

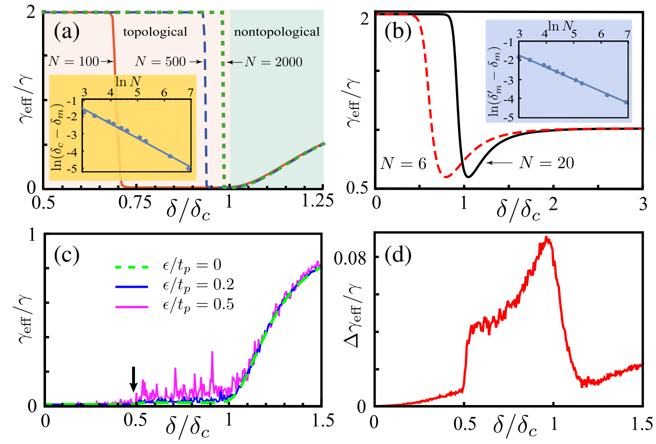

FIG. 4. (a) Superradiance-subradiance transition with different lattice lengths. The inset shows the finite-size scaling of SST for $\gamma_{AB} = 0.99\gamma$, where δ_m is defined by $\gamma_{\mathrm{eff}}(\delta_m) = \gamma$. (b) Effect of symmetry breaking resulting from waveguide-induced interactions between atoms, with $\gamma_{AB} = 0.97\gamma$ and the interactions between atoms in the same unit cells $g_{AB} = 0.1\gamma$. The inset shows the finite-size scaling behavior of $\ln(\delta'_m - \delta_m)$, where δ'_m indicates the SST in the symmetry-breaking case. (c) The effect of disorder in atomic frequencies, with $\gamma_{AB} = 0.99\gamma$ and $N = 50$. The arrow indicates the position $\delta = \delta_m$, where SST takes place. (d) The difference between averaged γ_{eff} with disorder ($\epsilon/t_p = 0.5$) and γ_{eff} without disorder. Other parameters for these figures: $t_c = t_p$, $\gamma = 10\kappa$.

transmission is versatile in detecting topological states [87–90]. Figure 3(b) shows the rescaled $\mathrm{Re}[\chi]$ (solid line) and $\mathrm{Im}[\chi]$ (dashed line) for both the left (green) and right (red) edge states. At $\delta = 0.1\delta_c$, as studied in Fig. 3(a), $\mathrm{Re}[\chi]$ is zero [see Fig. 3(b)]; therefore the transmission at resonance is $T_{\mathrm{res}} = 1/(1 + \mathrm{Im}[\chi]/\kappa)^2$. For the left (right) edge state, $\mathrm{Im}[\chi]/\kappa$ is 90 (0.45) and T_{res} is about 0 (0.48), for the given parameters. Figure 3(b) shows two regimes with different values of $\mathrm{Im}[\chi]$ in the topological phase, produced by a finite-size topological phase transition. The detailed physics will be discussed below.

Quantum coherence of topological superatom.—From the susceptibility, we can obtain the effective decay, $\gamma_{\mathrm{eff}} = -\mathrm{Im}(\Xi^{\intercal}\Xi/\chi)$ as in Refs. [91–93], of the topological superatom. Based on the coupling between light and edge states, we explore the quantum coherence, which can be inferred from γ_{eff} [94], in a topological superatom. We find that all the eigenmodes have the same coherence for $\gamma_{AB} = 0$. However, as shown in Figs. 3(c) and 3(d), the coherence properties of the superatom vary when δ is changed from the topological ($\delta < \delta_c$) to the nontopological ($\delta > \delta_c$) regime for nonzero γ_{AB}. In the topological regime, as shown in Fig. 3(d), we find the superradiance-subradiance transition (SST) by defining $\gamma_{\mathrm{eff}}(\delta_m) = \gamma$, where the transition point $\delta_m = 0.15\delta_c$ for given parameters characterizes the hybridization of the edge states. In the unhybridized regime $\delta < \delta_m$, the left edge state is subradiant ($\gamma_{\mathrm{eff},L} = \gamma - \gamma_{AB} < \gamma$), and the right edge state is superradiant ($\gamma_{\mathrm{eff},R} = \gamma + \gamma_{AB} > \gamma$). But, the hybridized edge states in the regime $\delta_m < \delta < \delta_c$ are subradiant, as shown in Figs. 3(c) and 3(d).

In Fig. 4(a), we further study the SST for different sizes of atom arrays. The inset presents the finite-size scaling behavior between the SST and the topological phase transition. The effective decay starts to increase after the topological phase transition. The symmetries in the atom array can be broken when waveguides induce interactions between atoms. In this scenario, the degeneracy of edge states is shifted, while the polarizations of edge states are preserved [64]. The SST is still found, as shown in Fig. 4(b). The inset shows the finite-size scaling behavior between SSTs for symmetry-breaking and symmetry-preserving cases. The shift of the SST produced by symmetry-breaking interactions depends on system's size. In Fig. 4(c), we study the disorder effect of atomic frequencies $\omega_{i\alpha} + \epsilon_{i\alpha}$ ($\alpha = A, B$), where the $\epsilon_{i\alpha}$ are randomly distributed $\epsilon_{i\alpha} \in [-\epsilon, \epsilon]$. Here, ϵ represents the strength of the disorder. The quantum coherence of the subradiant edge state without hybridization ($\delta < \delta_m$) is robust to random noise. However, the noise induces decoherence for hybridized edge states ($\delta_m < \delta < \delta_c$). In Fig. 4(d), we characterize the disorder-induced decoherence by $\Delta\gamma_{\mathrm{eff}} = \bar{\gamma_{\mathrm{eff}}} - \gamma_{\mathrm{eff}}$, where $\bar{\gamma_{\mathrm{eff}}}$ is the averaged effective decay of the disordered systems. The unhybridized subradiant edge state is indeed robust to noises, compared with the hybridized edge states and bulk states. It can be used for quantum memory.

Discussions and conclusions.—Recently, a ladder array with 24 superconducting artificial atoms has been experimentally demonstrated [95]. We find that even in small-size topological atom arrays realizable in current experiments, the collective edge states studied here can be observed. For example, when the number of unit cells is $N = 6$, the edge states are localized and allow for optical measurements [64]. The correlated decay $\gamma_{AB} = 0.99\gamma$ we considered in this work means a Purcell factor ~100, which has been realized in superconducting quantum circuits [84]. Moreover, by considering the fluctuations of atomic frequencies and interactions, we find that the quantum coherence of edge states can be robust to random noises [64].

In summary, we propose a quantum optical method to study topological matter. Owing to the large gaps between edge states and bulk states, a topological superatom is able to characterize the atom array in the low-energy regime. To optically drive the superatom, the unique properties of edge states (i.e., topology-protected polarization and boundary localization) are utilized. From the photon transmission, we find topology-protected quantum coherence distributed in the superatom. The topological superradiance and subradiance found here have important applications. When the symmetries in the system are preserved, the SST has a finite-size scaling relation with the topological critical point. This means that quantum coherence may provide an alternative way to characterize topological phases [96,97]. The SST is still found in symmetry-breaking systems, and the symmetry-breaking-induced shift of the SST depends on the system size. We study the effect of disorder on the system parameters and find that the quantum coherence of the unhybridized subradiant edge state is robust to random noises. Therefore, the superatom can be used as a topology-protected quantum memory. We hope that this proposal can be experimentally realized by a circuit-QED system.

The authors thank Xiong-Jun Liu, Jiang Zhang, and Ying Li for helpful discussions, and acknowledge Tao Liu and Yu-Ran Zhang for a critical reading. Y. X. L. is supported by the Key-Area Research and Development Program of GuangDong Province under Grant No. 2018B030326001, the National Basic Research Program (973) of China under Grant No. 2017YFA0304304 and NSFC under Grant No. 11874037. W. N. acknowledges the Tsinghua University Postdoctoral Support Program. Z. H. P. is supported by NSFC under Grant No. 61833010 and Hunan Province Science and Technology Innovation Platform and Talent Plan (Excellent Talent Award) under Grant No. 2017XK2021. F. N. is supported in part by the: MURI Center for Dynamic Magneto-Optics via the Air Force Office of Scientific Research (AFOSR) Grant No. FA9550-14-1-0040, Army Research Office (ARO) Grant No. W911NF-18-1-0358, Asian Office of Aerospace Research and Development (AOARD) Grant No. FA2386-18-1-4045, Japan Science and Technology Agency (JST) through the Q-LEAP program and CREST Grant No. JPMJCR1676, the Japan Society for the Promotion of Science (JSPS) through the JSPS-RFBR Grant No. 17-52-50023 and JSPS-FWO Grant No. VS.059.18N, the RIKEN-AIST Challenge Research Fund, the Foundational Questions Institute (FQXi), and the NTT Physics and Informatics (NTT-PHI) Laboratory.

*yuxiliu@mail.tsinghua.edu.cn

[1] M. Z. Hasan and C. L. Kane, Colloquium: Topological insulators, Rev. Mod. Phys. **82**, 3045 (2010).
[2] X.-L. Qi and S.-C. Zhang, Topological insulators and superconductors, Rev. Mod. Phys. **83**, 1057 (2011).
[3] K. Y. Bliokh, F. J. Rodríguez-Fortuño, F. Nori, and A. V. Zayats, Spin-orbit interactions of light, Nat. Photonics **9**, 796 (2015).
[4] T. Ozawa, H. M. Price, A. Amo, N. Goldman, M. Hafezi, L. Lu, M. Rechtsman, D. Schuster, J. Simon, O. Zilberberg, and I. Carusotto, Topological photonics, Rev. Mod. Phys. **91**, 015006 (2019).
[5] L.-J. Lang, X. Cai, and S. Chen, Edge States and Topological Phases in One-Dimensional Optical Superlattices, Phys. Rev. Lett. **108**, 220401 (2012).
[6] N. Goldman, J. Beugnon, and F. Gerbier, Detecting Chiral Edge States in the Hofstadter Optical Lattice, Phys. Rev. Lett. **108**, 255303 (2012).
[7] X. Li, E. Zhao, and W. V. Liu, Topological states in a ladder-like optical lattice containing ultracold atoms in higher orbital bands, Nat. Commun. **4**, 1523 (2013).
[8] A. Y. Kitaev, Unpaired majorana fermions in quantum wires, Phys. Usp. **44**, 131 (2001).
[9] J. Q. You, X.-F. Shi, X. Hu, and F. Nori, Quantum emulation of a spin system with topologically protected ground states using superconducting quantum circuits, Phys. Rev. B **81**, 014505 (2010).
[10] J. Alicea, Y. Oreg, G. Refael, F. von Oppen, and M. P. A. Fisher, Non-Abelian statistics and topological quantum information processing in 1D wire networks, Nat. Phys. **7**, 412 (2011).
[11] X.-J. Liu, Z.-X. Liu, and M. Cheng, Manipulating Topological Edge Spins in a One-Dimensional Optical Lattice, Phys. Rev. Lett. **110**, 076401 (2013).
[12] J. Q. You, Z. D. Wang, W. X. Zhang, and F. Nori, Encoding a qubit with Majorana modes in superconducting circuits, Sci. Rep. **4**, 5535 (2015).
[13] N. Y. Yao, C. R. Laumann, A. V. Gorshkov, H. Weimer, L. Jiang, J. I. Cirac, P. Zoller, and M. D. Lukin, Topologically protected quantum state transfer in a chiral spin liquid, Nat. Commun. **4**, 1585 (2013).
[14] C. Dlaska, B. Vermersch, and P. Zoller, Robust quantum state transfer via topologically protected edge channels in dipolar arrays, Quantum Sci. Technol. **2**, 015001 (2017).
[15] K. Y. Bliokh, D. Smirnova, and F. Nori, Quantum spin Hall effect of light, Science **348**, 1448 (2015).
[16] K. Y. Bliokh, D. Leykam, M. Lein, and F. Nori, Topological non-Hermitian origin of surface Maxwell waves, Nat. Commun. **10**, 580 (2019).
[17] P. St-Jean, V. Goblot, E. Galopin, A. Lemaître, T. Ozawa, L. Le Gratiet, I. Sagnes, J. Bloch, and A. Amo, Lasing in

topological edge states of a one-dimensional lattice, Nat. Photonics **11**, 651 (2017).
[18] B. Bahari, A. Ndao, F. Vallini, A. E. Amili, Y. Fainman, and B. Kanté, Nonreciprocal lasing in topological cavities of arbitrary geometries, Science **358**, 636 (2017).
[19] G. Harari, M. A. Bandres, Y. Lumer, M. C. Rechtsman, Y. D. Chong, M. Khajavikhan, D. N. Christodoulides, and M. Segev, Topological insulator laser: Theory, Science **359**, eaar4003 (2018).
[20] M. A. Bandres, S. Wittek, G. Harari, M. Parto, J. Ren, M. Segev, D. N. Christodoulides, and M. Khajavikhan, Topological insulator laser: Experiments, Science **359**, eaar4005 (2018).
[21] J. Perczel, J. Borregaard, D. E. Chang, H. Pichler, S. F. Yelin, P. Zoller, and M. D. Lukin, Topological Quantum Optics in Two-Dimensional Atomic Arrays, Phys. Rev. Lett. **119**, 023603 (2017).
[22] J.-S. Pan, X.-J. Liu, W. Zhang, W. Yi, and G.-C. Guo, Topological Superradiant States in a Degenerate Fermi Gas, Phys. Rev. Lett. **115**, 045303 (2015).
[23] F. Mivehvar, H. Ritsch, and F. Piazza, Superradiant Topological Peierls Insulator inside an Optical Cavity, Phys. Rev. Lett. **118**, 073602 (2017).
[24] P. Doyeux, S. A. H. Gangaraj, G. W. Hanson, and M. Antezza, Giant Interatomic Energy-Transport Amplification with Nonreciprocal Photonic Topological Insulators, Phys. Rev. Lett. **119**, 173901 (2017).
[25] S. Barik, A. Karasahin, C. Flower, T. Cai, H. Miyake, W. DeGottardi, M. Hafezi, and E. Waks, A topological quantum optics interface, Science **359**, 666 (2018).
[26] R. H. Dicke, Coherence in spontaneous radiation processes, Phys. Rev. **93**, 99 (1954).
[27] M. O. Scully, Collective Lamb Shift in Single Photon Dicke Superradiance, Phys. Rev. Lett. **102**, 143601 (2009).
[28] M. O. Scully, Single Photon Subradiance: Quantum Control of Spontaneous Emission and Ultrafast Readout, Phys. Rev. Lett. **115**, 243602 (2015).
[29] P. Tighineanu, R. S. Daveau, T. B. Lehmann, H. E. Beere, D. A. Ritchie, P. Lodahl, and S. Stobbe, Single-Photon Superradiance from a Quantum Dot, Phys. Rev. Lett. **116**, 163604 (2016).
[30] S. J. Roof, K. J. Kemp, M. D. Havey, and I. M. Sokolov, Observation of Single-Photon Superradiance and the Cooperative Lamb Shift in an Extended Sample of Cold Atoms, Phys. Rev. Lett. **117**, 073003 (2016).
[31] L. Chen, P. Wang, Z. Meng, L. Huang, H. Cai, D.-W. Wang, S.-Y. Zhu, and J. Zhang, Experimental Observation of One-Dimensional Superradiance Lattices in Ultracold Atoms, Phys. Rev. Lett. **120**, 193601 (2018).
[32] V. Vuletic, When superatoms talk photons, Nat. Phys. **2**, 801 (2006).
[33] R. Heidemann, U. Raitzsch, V. Bendkowsky, B. Butscher, R. Löw, L. Santos, and T. Pfau, Evidence for Coherent Collective Rydberg Excitation in the Strong Blockade Regime, Phys. Rev. Lett. **99**, 163601 (2007).
[34] A. Paris-Mandoki, C. Braun, J. Kumlin, C. Tresp, I. Mirgorodskiy, F. Christaller, H. P. Büchler, and S. Hofferberth, Free-Space Quantum Electrodynamics with a Single Rydberg Superatom, Phys. Rev. X **7**, 041010 (2017).
[35] Y. Bahri, R. Vosk, E. Altman, and A. Vishwanath, Localization and topology protected quantum coherence at the edge of hot matter, Nat. Commun. **6**, 7341 (2015).
[36] L. C. Venuti, Z. Ma, H. Saleur, and S. Haas, Topological protection of coherence in a dissipative environment, Phys. Rev. A **96**, 053858 (2017).
[37] J. Kemp, N. Y. Yao, C. R. Laumann, and P. Fendley, Long coherence times for edge spins, J. Stat. Mech. 2017, 063105 (2017).
[38] I.-D. Potirniche, A. C. Potter, M. Schleier-Smith, A. Vishwanath, and N. Y. Yao, Floquet Symmetry-Protected Topological Phases in Cold-Atom Systems, Phys. Rev. Lett. **119**, 123601 (2017).
[39] P. Milman, W. Maineult, S. Guibal, L. Guidoni, B. Douçot, L. Ioffe, and T. Coudreau, Topologically Decoherence-Protected Qubits with Trapped Ions, Phys. Rev. Lett. **99**, 020503 (2007).
[40] C. Nayak, S. H. Simon, A. Stern, M. Freedman, and S. D. Sarma, Non-Abelian anyons and topological quantum computation, Rev. Mod. Phys. **80**, 1083 (2008).
[41] S. Diehl, E. Rico, M. A. Baranov, and P. Zoller, Topology by dissipation in atomic quantum wires, Nat. Phys. **7**, 971 (2011).
[42] Z.-Y. Xue, S.-L. Zhu, J. Q. You, and Z. D. Wang, Implementing topological quantum manipulation with superconducting circuits, Phys. Rev. A **79**, 040303(R) (2009).
[43] M. Trif and Y. Tserkovnyak, Resonantly Tunable Majorana Polariton in a Microwave Cavity, Phys. Rev. Lett. **109**, 257002 (2012).
[44] T. L. Schmidt, A. Nunnenkamp, and C. Bruder, Majorana Qubit Rotations in Microwave Cavities, Phys. Rev. Lett. **110**, 107006 (2013).
[45] M. C. Dartiailh, T. Kontos, B. Douçot, and A. Cottet, Direct Cavity Detection of Majorana Pairs, Phys. Rev. Lett. **118**, 126803 (2017).
[46] M. König, S. Wiedmann, C. Brüne, A. Roth, H. Buhmann, L. W. Molenkamp, X.-L. Qi, and S.-C. Zhang, Quantum spin hall insulator state in HgTe quantum wells, Science **318**, 766 (2007).
[47] D. Hsieh, Y. Xia, D. Qian, L. Wray, J. H. Dil, F. Meier, J. Osterwalder, L. Patthey, J. G. Checkelsky, N. P. Ong, A. V. Fedorov, H. Lin, A. Bansil, D. Grauer, Y. S. Hor, R. J. Cava, and M. Z. Hasan, A tunable topological insulator in the spin helical Dirac transport regime, Nature (London) **460**, 1101 (2009).
[48] Z. Wang, Y. Chong, J. D. Joannopoulos, and M. Soljačić, Observation of unidirectional backscattering-immune topological electromagnetic states, Nature (London) **461**, 772 (2009).
[49] M. Hafezi, E. A. Demler, M. D. Lukin, and J. M. Taylor, Robust optical delay lines with topological protection, Nat. Phys. **7**, 907 (2011).
[50] C.-Z. Chang *et al.*, Experimental observation of the quantum anomalous Hall effect in a magnetic tpological insulator, Science **340**, 167 (2013).
[51] I. Buluta, S. Ashhab, and F. Nori, Natural and artificial atoms for quantum computation, Rep. Prog. Phys. **74**, 104401 (2011).
[52] X. Gu, A. F. Kockum, A. Miranowicz, Y.-X. Liu, and F. Nori, Microwave photonics with superconducting quantum circuits, Phys. Rep. **718–719**, 1 (2017).

[53] J. H. Béjanin, T. G. McConkey, J. R. Rinehart, C. T. Earnest, C. R. H. McRae, D. Shiri, J. D. Bateman, Y. Rohanizadegan, B. Penava, P. Breul, S. Royak, M. Zapatka, A. G. Fowler, and M. Mariantoni, Three-Dimensional Wiring for Extensible Quantum Computing: The Quantum Socket, Phys. Rev. Applied **6**, 044010 (2016).

[54] Q. Liu, M. Li, K. Dai, K. Zhang, G. Xue, X. Tan, H. Yu, and Y. Yu, Extensible 3D architecture for superconducting quantum computing, Appl. Phys. Lett. **110**, 232602 (2017).

[55] D. Rosenberg, D. Kim, R. Das, D. Yost, S. Gustavsson, D. Hover, P. Krantz, A. Melville, L. Racz, G. O. Samach, S. J. Weber, F. Yan, J. L. Yoder, A. J. Kerman, and W. D. Oliver, 3D integrated superconducting qubits, Quantum Inf. **3**, 42 (2017).

[56] A. Dunsworth *et al.*, A method for building low loss multi-layer wiring for superconducting microwave devices, Appl. Phys. Lett. **112**, 063502 (2018).

[57] Z. Chen, A. Megrant, J. Kelly, R. Barends, J. Bochmann, Y. Chen, B. Chiaro, A. Dunsworth, E. Jeffrey, J. Y. Mutus, P. J. J. O'Malley, C. Neill, P. Roushan, D. Sank, A. Vainsencher, J. Wenner, T. C. White, A. N. Cleland, and J. M. Martinis, Fabrication and characterization of aluminum airbridges for superconducting microwave circuits, Appl. Phys. Lett. **104**, 052602 (2014).

[58] H. Mukai, K. Sakata, S. J. Devitt, R. Wang, Y. Zhou, Y. Nakajima, and J. S. Tsai, Pseudo-2D superconducting quantum computing circuit for the surface code, arXiv:1902.07911.

[59] D. Rosenberg, S. Weber, D. Conway, D. Yost, J. Mallek, G. Calusine, R. Das, D. Kim, M. Schwartz, W. Woods, J. L. Yoder, and W. D. Oliver, 3D integration and packaging for solid-state qubits, arXiv:1906.11146.

[60] S.-B. Zheng and G.-C. Guo, Efficient Scheme for Two-Atom Entanglement and Quantum Information Processing in Cavity QED, Phys. Rev. Lett. **85**, 2392 (2000).

[61] S. Osnaghi, P. Bertet, A. Auffeves, P. Maioli, M. Brune, J. M. Raimond, and S. Haroche, Coherent Control of an Atomic Collision in a Cavity, Phys. Rev. Lett. **87**, 037902 (2001).

[62] J. Majer, J. M. Chow, J. M. Gambetta, J. Koch, B. R. Johnson, J. A. Schreier, L. Frunzio, D. I. Schuster, A. A. Houck, A. Wallraff, A. Blais, M. H. Devoret, S. M. Girvin, and R. J. Schoelkopf, Coupling superconducting qubits via a cavity bus, Nature (London) **449**, 443 (2007).

[63] R. E. Evans, M. K. Bhaskar, D. D. Sukachev, C. T. Nguyen, A. Sipahigil, M. J. Burek, B. Machielse, G. H. Zhang, A. S. Zibrov, E. Bielejec, H. Park, M. Lončar, and M. D. Lukin, Photon-mediated interactions between quantum emitters in a diamond nanocavity, Nature (London) **362**, 662 (2018).

[64] See Supplemental Material at http://link.aps.org/supplemental/10.1103/PhysRevLett.124.023603 for additional details about 3D integrated superconducting quantum circuits, effective Hamiltonian, edge states, driving the topological superatom in a cavity, and the effects of symmetry breaking and disorder.

[65] V. D. Vaidya, Y. Guo, R. M. Kroeze, K. E. Ballantine, A. J. Kollár, J. Keeling, and B. L. Lev, Tunable-Range, Photon-Mediated Atomic Interactions in Multimode Cavity QED, Phys. Rev. X **8**, 011002 (2018).

[66] K. Xu, J.-J. Chen, Y. Zeng, Y.-R. Zhang, C. Song, W. Liu, Q. Guo, P. Zhang, D. Xu, H. Deng, K. Huang, H. Wang, X. Zhu, D. Zheng, and H. Fan, Emulating Many-Body Localization with a Superconducting Quantum Processor, Phys. Rev. Lett. **120**, 050507 (2018).

[67] M. A. Norcia, R. J. Lewis-Swan, J. R. K. Cline, B. Zhu, A. M. Rey, and J. K. Thompson, Cavity-mediated collective spin-exchange interactions in a strontium superradiant laser, Science **361**, 259 (2018).

[68] S. Ryu and Y. Hatsugai, Topological Origin of Zero-Energy Edge States in Particle-Hole Symmetric Systems, Phys. Rev. Lett. **89**, 077002 (2002).

[69] A. P. Schnyder, S. Ryu, A. Furusaki, and A. W. W. Ludwig, Classification of topological insulators and superconductors in three spatial dimensions, Phys. Rev. B **78**, 195125 (2008).

[70] G. Zhang and Z. Song, Topological Characterization of Extended Quantum Ising Models, Phys. Rev. Lett. **115**, 177204 (2015).

[71] T. Liu, Y.-R. Zhang, Q. Ai, Z. Gong, K. Kawabata, M. Ueda, and F. Nori, Second-Order Topological Phases in Non-Hermitian Systems, Phys. Rev. Lett. **122**, 076801 (2019).

[72] M. König, H. Buhmann, L. W. Molenkamp, T. Hughes, C.-X. Liu, X.-L. Qi, and S.-C. Zhang, The quantum spin Hall effect: Theory and experiment, J. Phys. Soc. Jpn. **77**, 031007 (2008).

[73] É. Dumur, B. Küng, A. K. Feofanov, T. Weissl, N. Roch, C. Naud, W. Guichard, and O. Buisson, V-shaped superconducting artificial atom based on two inductively coupled transmons, Phys. Rev. B **92**, 020515 (2015).

[74] P.-O. Guimond, H. Pichler, A. Rauschenbeutel, and P. Zoller, Chiral quantum optics with V-level atoms and coherent quantum feedback, Phys. Rev. A **94**, 033829 (2016).

[75] N. Shammah, S. Ahmed, N. Lambert, S. D. Liberato, and F. Nori, Open quantum systems with local and collective incoherent processes: Efficient numerical simulations using permutational invariance, Phys. Rev. A **98**, 063815 (2018).

[76] G. S. Agarwal, in *Quantum Statistical Theories of Spontaneous Emission and Their Relation to Other Approaches*, edited by G. Höhler, Springer Tracts in Modern Physics Vol. 70 (Springer, Berlin, 1974).

[77] P. Zhou and S. Swain, Ultranarrow Spectral Lines via Quantum Interference, Phys. Rev. Lett. **77**, 3995 (1996).

[78] S.-Y. Zhu and M. O. Scully, Spectral Line Elimination and Spontaneous Emission Cancellation via Quantum Interference, Phys. Rev. Lett. **76**, 388 (1996).

[79] G. S. Agarwal, Anisotropic Vacuum-Induced Interference in Decay Channels, Phys. Rev. Lett. **84**, 5500 (2000).

[80] Y. P. Yang, J. P. Xu, and S. Y. Zhu, Quantum Interference Enhancement with Left-Handed Materials, Phys. Rev. Lett. **100**, 043601 (2008).

[81] S. Das, G. S. Agarwal, and M. O. Scully, Quantum Interferences in Cooperative Dicke Emission from Spatial Variation of the Laser Phase, Phys. Rev. Lett. **101**, 153601 (2008).

[82] A. Gonzalez-Tudela, D. Martin-Cano, E. Moreno, L. Martin-Moreno, C. Tejedor, and F. J. Garcia-Vidal, Entanglement of Two Qubits Mediated by One-Dimensional Plasmonic Waveguides, Phys. Rev. Lett. **106**, 020501 (2011).

[83] A. F. van Loo, A. Fedorov, K. Lalumière, B. C. Sanders, A. Blais, and A. Wallraff, Photon-mediated interactions between distant artificial atoms, Science **342**, 1494 (2013).

[84] M. Mirhosseini, E. Kim, X. Zhang, A. Sipahigil, P. B. Dieterle, A. J. Keller, A. Asenjo-Garcia, D. E. Chang, and O. Painter, Cavity quantum electrodynamics with atom-like mirrors, Nature (London) **569**, 692 (2019).

[85] J. McKeever, A. Boca, A. D. Boozer, J. R. Buck, and H. J. Kimble, Experimental realization of a one-atom laser in the regime of strong coupling, Nature (London) **425**, 268 (2003).

[86] O. Astafiev, A. M. Zagoskin, A. A. Abdumalikov, Jr., Y. A. Pashkin, T. Yamamoto, K. Inomata, Y. Nakamura, and J. S. Tsai, Resonance fluorescence of a single artificial atom, Science **327**, 840 (2010).

[87] X.-J. Liu, X. Liu, C. Wu, and J. Sinova, Quantum anomalous Hall effect with cold atoms trapped in a square lattice, Phys. Rev. A **81**, 033622 (2010).

[88] M. C. Rechtsmann, J. M. Zeuner, Y. Plotnik, Y. Lumer, D. Podolsky, F. Dreisow, S. Nolte, M. Segev, and A. Szameit, Photonic Floquet topological insulators, Nature (London) **496**, 196 (2013).

[89] M. Xiao, Z. Q. Zhang, and C. T. Chan, Surface Impedance and Bulk Band Geometric Phases in One-Dimensional Systems, Phys. Rev. X **4**, 021017 (2014).

[90] F. Mei, J.-B. You, W. Nie, R. Fazio, S.-L. Zhu, and L. C. Kwek, Simulation and detection of photonic Chern insulators in a one-dimensional circuit-QED lattice, Phys. Rev. A **92**, 041805(R) (2015).

[91] K. Kakuyanagi, Y. Matsuzaki, C. Déprez, H. Toida, K. Semba, H. Yamaguchi, W. J. Munro, and S. Saito, Observation of Collective Coupling between an Engineered Ensemble of Macroscopic Artificial Atoms and a Superconducting Resonator, Phys. Rev. Lett. **117**, 210503 (2016).

[92] D. Plankensteiner, C. Sommer, H. Ritsch, and C. Genes, Cavity Antiresonance Spectroscopy of Dipole Coupled Subradiant Arrays, Phys. Rev. Lett. **119**, 093601 (2017).

[93] A. Albrecht, L. Henriet, A. Asenjo-Garcia, P. B. Dieterle, O. Painter, and D. E. Chang, Subradiant states of quantum bits coupled to a one-dimensional waveguide, New J. Phys. **21**, 025003 (2019).

[94] A. Zhang, K. Zhang, L. Zhou, and W. Zhang, Frozen Condition of Quantum Coherence for Atoms on a Stationary Trajectory, Phys. Rev. Lett. **121**, 073602 (2018).

[95] Y. Ye *et al.*, Propagation and Localization of Collective Excitations on a 24-Qubit Superconducting Processor, Phys. Rev. Lett. **123**, 050502 (2019).

[96] L. Pezzè, M. Gabbrielli, L. Lepori, and A. Smerzi, Multipartite Entanglement in Topological Quantum Phases, Phys. Rev. Lett. **119**, 250401 (2017).

[97] Y.-R. Zhang, Y. Zeng, H. Fan, J. Q. You, and F. Nori, Characterization of Topological States via Dual Multipartite Entanglement, Phys. Rev. Lett. **120**, 250501 (2018).